Multi-Path Measurements Using a 1.3 GHz Radar Signal Received by the GBT

J. R. Fisher, NRAO, Green Bank, WV 24944
rfisher@nrao.edu

Introduction

Any technique for removing radio frequency interference (RFI) from radio astronomy data must take into account modifications to the interfering signal by propagation conditions between the transmitter and the radio telescope. In particular, a signal may arrive by way of several propagation paths, which can have considerable differences in delay and direction of arrival. This paper describes an initial study of a radar signal received by the Green Bank Telescope (GBT) from an air surveillance radar transmitter 104 kilometers south-southwest of the telescope. Radar is especially useful for propagation studies because it transmits short pulses in a narrow beam which sweeps in azimuth.

The radar studied was an ARSR-3 Air Surveillance Radar transmitting at 1292.01 MHz. The pulse length was 2 microseconds with an average repetition rate of about 340 Hz. The azimuth sweep rate was 5 revolutions per minute, and the azimuthal beamwidth was approximately 1 degree. The pulse transmission times varied by 100-microsecond increments from a constant interval in a repeating sequence of [0, 4, 0, 3, 1, 2, 1, 3]. A 10 MHz bandwidth baseband signal was recorded at 20 megasamples per second with an 8-bit sampler. The radar carrier appeared in the baseband spectrum at about 5.8 MHz. The data spanned a 5-second period beginning about 1.1 seconds before the radar beam passed over the GBT.

Pulse Signature

A typical pulse signature sampled by the 8-bit A/D converter is shown in Figure 1. The pulse was distorted somewhat by the long propagation path of

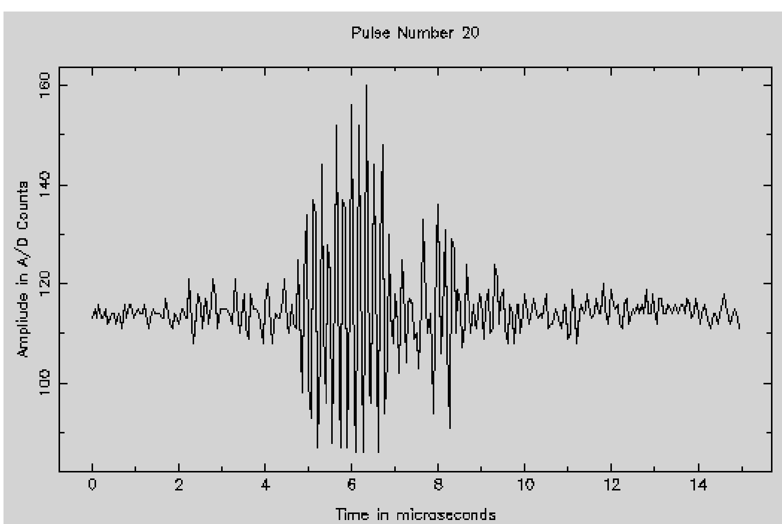

Figure 1. Pulse signature sampled by the A/D converter.

104 km. A weaker delayed pulse can be seen about 3 microseconds after the main pulse, due to scattering near the GBT.

The pulse shown in Figure 1 was recorded when the radar beam was several beamwidths away from the direction of Green Bank. The GBT receiver was saturated by pulses received when the beam passed over the GBT. Even at their strongest, the pulses did not appear to blind the receiver. They just caused clipping of the waveform peaks.

Pulse Filter

Better pulse sensitivity was obtained by convolving the data with a function that closely matched the pulse signature. An approximation to a pulse filter

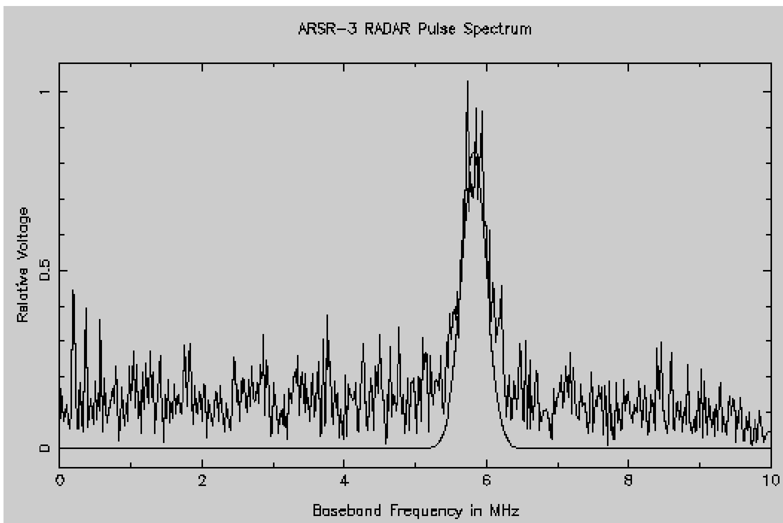

Figure 2. Gaussian fit to a pulse spectrum for the purpose of deriving a pulse convolution function.

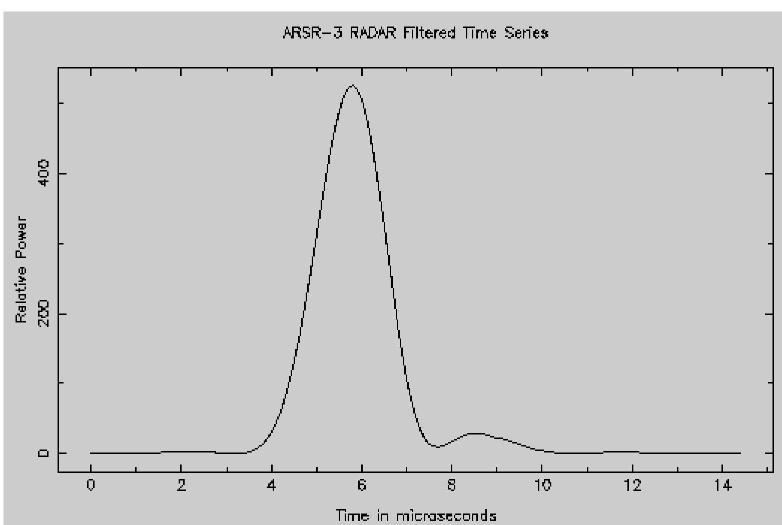

Figure 3. Pulse in Figure 1 filtered by the function shown in Figure 2.

was derived by a rough fit of a gaussian curve to the power spectrum of the pulse as shown in Figure 2.

The data were broken into 64 kB blocks, Fourier transformed, multiplied by the frequency domain filter function, and the transformed back to the time domain. The convolved time series of the pulse shown in Figure 1, squared to get power as a function of time, then looks like the data in Figure 3. The filter function can probably be tuned a bit for a better balance between signal-to-noise ratio and pulse resolution.

Pulse Arrival Times

All 5 seconds of the data were then filtered and searched for identifiable separate pulses above most of the highest random noise peaks. The differences between expected and measured pulse arrival times are shown in Figure 4. The first part of the data run was found to have a constant pulse arrival time by assuming a pulse repetition rate of 341.4142 pulses per second. The drift in arrival times toward the end of the 5 seconds of data was due to either a drift in the radar timing generator or the internal clock of our data acquisition board of about 60 parts per million in frequency. This drift was removed empirically with a polynomial time correction function fitted by eye to the arrival times.

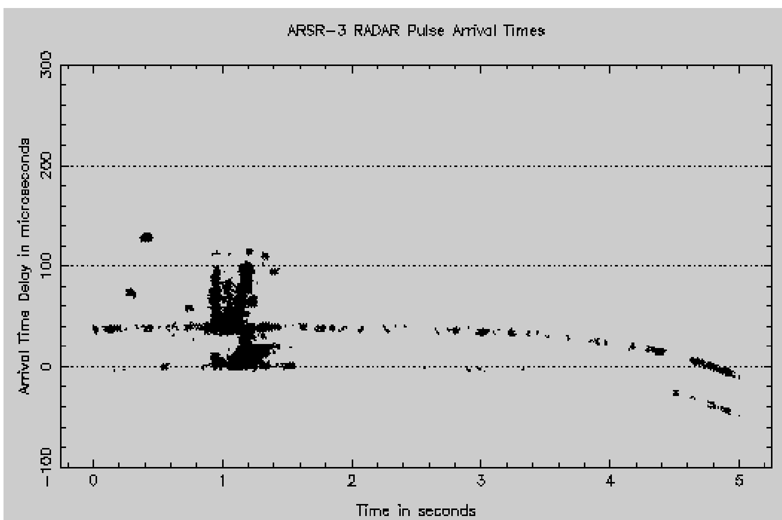

Figure 4. Pulse arrival time delays for the full data set.

At least three features in Figure 4 stand out. First, pulses at a constant delay of about 35 microseconds were present during the full length of the data set. This is due to the fact that we saw pulses from the radar even when the radar beam was pointed well away from Green Bank. Since the receiver saturated with the beam pointed in our direction, we cannot determine the relative strengths of the sidelobes, but they were at least 30 dB below the main beam.

The second notable feature of Figure 4 is that the earliest pulses were not the most prevalent. The shortest distance, great circle, diffraction path from the radar to the GBT must have produced the earliest arriving pulses.

Evidently a longer path had a lower propagation loss since the pulses from the radar antenna sidelobes were most apparent at an extra delay of about 35 microseconds. The plots below will show that this lower propagation loss was produced by a reflection from the high mountain ridge about 8 km west of the GBT. A great circle plot of the terrain profile in the direction of the radar shows that the GBT is about 400 meters below the elevation of the nearest diffraction obstacle about 12 km away. The mountain ridge west of the GBT includes Bald Knob, the second highest peak in West Virginia.

The third notable feature of Figure 4 is the cluster of pulses around 1.1 seconds into the data sample. This was the time when the radar beam passed over Green Bank, and we saw reflections from local terrain features in addition to the directly arriving pulse.

Geometric interpretation of Arrival Times

The pulse delay can be interpreted as a physical location of the reflecting object by assuming that only one reflection is involved. The reflection point is then the intersection of three surfaces: the locus of constant delay, which is an ellipsoid with the GBT and the radar antenna at the focii; the vertical plane of the radar beam; and the horizontal plane at the assumed altitude of the reflector. Figure 5 is a map of the intersection point solutions for all of the pulse delays shown in Figure 4, assuming that the reflector altitude is the same as the altitude of the GBT.

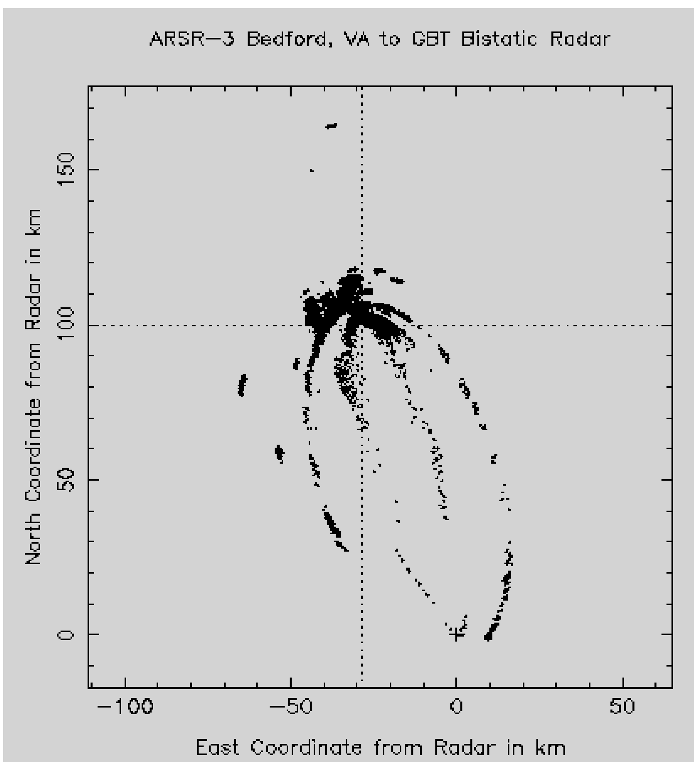

Figure 5. Reflection point locations computed from pulse arrival delays and the radar beam azimuth. The GBT is at the intersection of the two long dotted lines, and the radar is at the small cross near the bottom of the diagram. The radar azimuth sweep during the 5-second data set is from about 325 to 115 degrees.

The heavy ellipse in Figure 5 is the locus of constant delay of about 35 microseconds due to pulses from the radar antenna sidelobes reflected from the ridge west of the GBT. The weaker inner ellipse is the near-zero-delay locus of the direct path from the radar to the GBT. The cluster of points to the northwest of the GBT corresponds to high terrain in this direction. Other features could be either terrain reflections or aircraft in the area. The small cluster farthest north is almost certainly from an aircraft.

Figure 6 is an expanded plot of the strongest pulses from the area northwest of the GBT. These pulses were more than ten times the intensity of the weakest pulses shown in Figure 5. The band of points running from the lower left corner of Figure 6 to the top center corresponds to the ridge of high peaks shown in the contour map of Figure 7. The scales of the two maps in Figures 6 and 7 are about the same. An accurate overlay of the radar returns on the contour map shows that the three clusters of points near the top of Figure 6 coincide nicely to the individual peaks on the ridge.

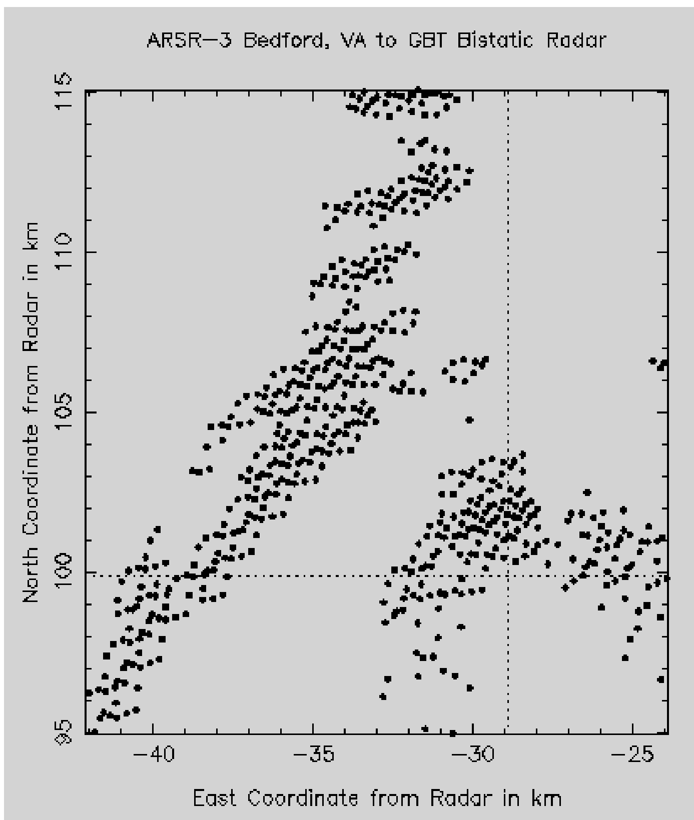

Figure 6. The geometric interpretation of the delays of the strongest pulses received from locations to the immediate northwest of the GBT.

Since the azimuth of the radar beam and the pulse delay zero point must be inferred from the data, these are two free parameters that were empirically determined by fitting the point locations in Figure 6 to terrain features in Figure 7. The match of returns to mountain peaks appears pretty convincing, but keep in mind that this is not based on accurate zero-point calibrations.

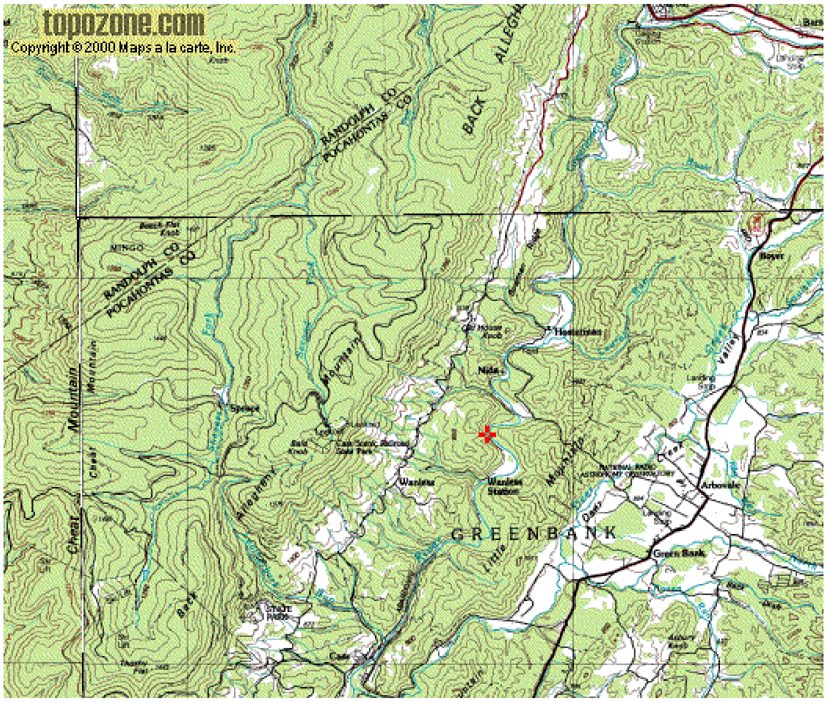

Figure 7. Contour map of the terrain to the west and north of Green Bank. The GBT is located slightly to the northeast of the 'K' in the large word "GREENBANK" and below the small print "National Radio Astronomy Observatory."

Pulse Intensity Distribution

Relatively strong pulses were seen to be coming from a number of reflection points in the terrain around the GBT so there was not a completely dominant reflection point. Figure 8 shows the pulse intensity as a function of delay. A directly arriving pulse had a delay of zero. The pulses at about 43 microseconds saturated the GBT receiver so these were probably 10 to 20 dB higher than measured. The pulses around 5 microseconds delay may also have

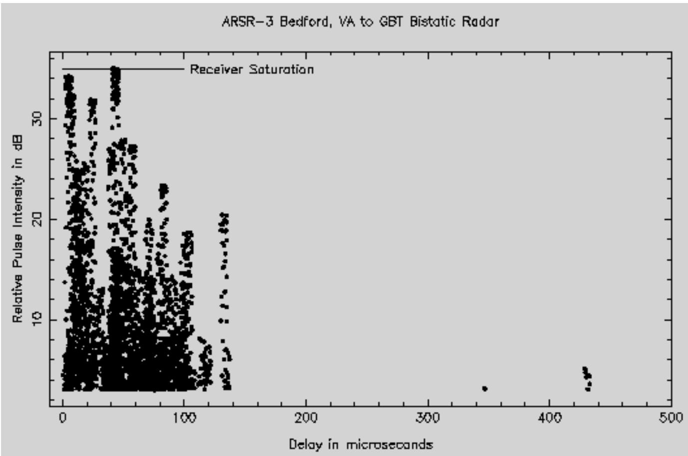

Figure 8. Pulse intensity as a function of delay from the pulse arriving directly from the radar for the data set shown in Figures 4, 5, and 6.

been saturated but not as severely. Quite strong pulses can be seen out to a delay of 135 microseconds. Most, if not all delayed pulses were from terrain reflections. The group of returns at 430 microseconds is probably from an aircraft.

Figure 9 shows the measured pulse intensities as a function of computed azimuth as seen from the GBT of the reflection points for pulses with delays greater than 50 microseconds. This delay cutoff eliminates the pulses coming from the radar antenna sidelobes that appear to be smeared over a wide range of azimuths as seen in Figure 5. Hence, the directly arriving pulses and the strongest reflected pulses are not shown in Figure 9. The strongest reflection not in this figure is from an azimuth of about -75 degrees.

Because of the large distance to the radar antenna, the azimuth resolution from the GBT is not terribly good, but the wide distribution of azimuths seen in Figure 9 is real. The azimuth profile of a single reflection point can be seen from the paraboloid-like arcs of points. More distant reflections from the GBT have narrower arcs.

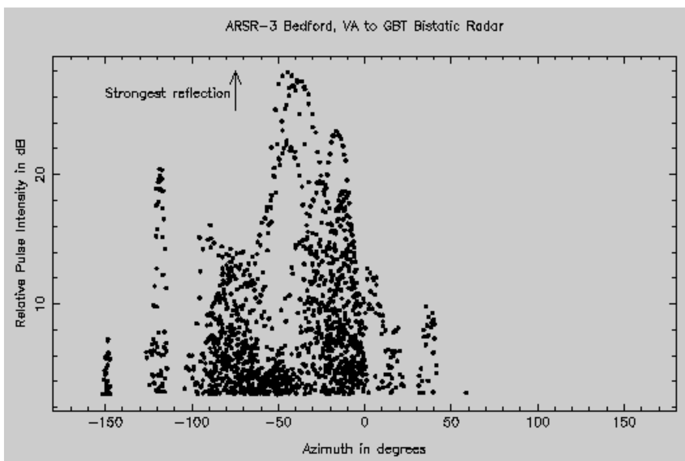

Figure 9. Pulse intensity as a function of inferred azimuth of the radar pulse reflection point as seen from the GBT for pulses with delays greater than 50 microseconds for the data set shown in Figures 4, 5, 6, and 8. Zero azimuth is north and +90 degrees is east.

Time Window Blanking

Two straightforward blanking techniques were tried on the data set, time window blanking and detected pulse blanking, to determine whether the radar signal can be effectively removed from the spectrum.

In the tests that follow spectra were integrated over chosen intervals in the data by forming spectra with FFT's of overlapping 2048-data-sample sets and accumulating the power spectra. The data-sample sets overlapped by 50% (1024 samples) to reduce the sensitivity loss due to missing correlations between adjacent sample sets. Time window blanking was implemented by not accumulating spectra that had any of their input data extending into the time interval to be blanked.

Figure 10 shows the unblanked spectrum accumulated over the 0.3-second interval when the radar beam was closest to the Green Bank azimuth.

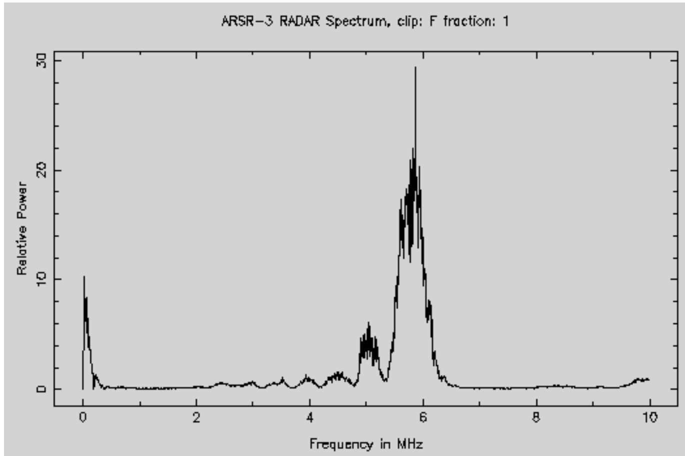

Figure 10. Unblanked spectrum integrated over to time when the radar beam was sweeping over the GBT, between 0.95 and 1.25 seconds into the data. The intensity scale is in units of telescope system noise power.

Figure 11 shows the spectrum accumulated over this same interval but with time window blanking beginning 20 microseconds before and ending 150 microseconds after the first pulses arrive from the radar. About 10% of the spectra were rejected in this integration. This time window can be compared with the time distribution of pulses shown in Figure 8. Figure 11 shows that even with a few weak pulses from aircraft reflections around 430 microseconds included in the spectrum, no trace of the radar signal can be seen. The reference spectrum used to normalize the data in Figures 10 and 11 was an accumulation of spectra over the full 5-second data set that fell outside of a time window from 20 microseconds before to 500 microseconds after the first-arriving pulses. The rms noise amplitude is about what is expected for a 0.3-second integration and 10-kHz spectral resolution.

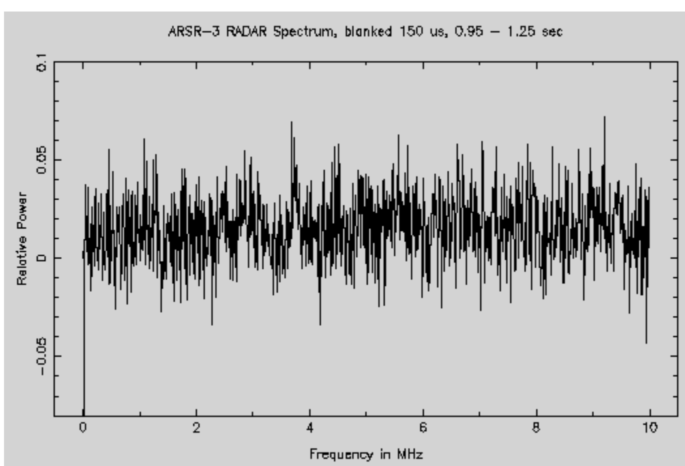

Figure 11. Spectrum with data blanked for 150 microseconds after the earliest arriving pulses. The spectrum was integrated between 0.95 and 1.25 seconds into the data as in Figure 10. The intensity scale is in units of telescope system noise power.

The robustness of the time window blanking was tested by reducing the blanking window width to include more radar pulses in the integration. Evidence of a radar spectral feature did not show up until the end of the blanking window was reduced to about 100 microseconds after the first-arriving pulse. In Figure 8 you can see that quite a few moderately strong pulses beyond 110 microseconds could be included without distorting the spectrum. Of course, an integration over many radar rotation periods would uncover the spectral signature of these pulses so they do need to be blanked.

Integration of spectra over the full 12-second interval of the radar sweep still needs to reject the weak pulses from the radar antenna sidelobes, as will be shown below. However, these spectra will tend to dilute any residual radar signal coming from pulses outside of the blanking time window. The rejection tests associated with Figure 11 are about the most stringent that we can make with the present data.

Detected Pulse Blanking

We could avoid the problem of continuously measuring radar pulse arrival times to microsecond accuracy to synchronize a blanking window by simply throwing away spectra that contain a detected pulse. To test the effectiveness of this scheme we started with the unblanked spectrum integrated when the radar beam is not pointed very close to the GBT as shown in Figure 12. The fact that we see the radar spectral signature in this spectrum says that we cannot simply blank our spectrometer when the radar beam is pointed near the direction of the GBT.

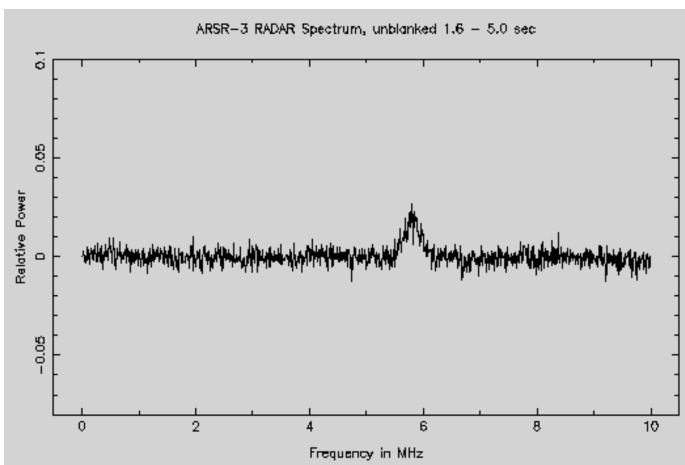

Figure 12. Unblanked spectrum integrated over to time when the radar beam was pointed away from the GBT, between 1.6 and 5 seconds into the data. The intensity scale is in units of telescope system noise power.

When we rejected all spectra in which we detected a radar pulse with an amplitude greater than 1.5, using the same pulse filtering techniques described above, we get the spectrum shown in Figure 13. Only about 0.4% of the spectra were rejected, and little, if any improvement can be seen in the blanked spectrum. Figure 14 shows the number distribution of measured pulse amplitudes near the tail of the random noise distribution. Further reduction of the rejected pulse cutoff will reject a rapidly increasing fraction of spectra due to random noise. An artificial hole in the spectrum can be created with random noise rejection because spectra with noise peaks at the filtered frequency will be selectively thrown out. Hence, this pulse rejection scheme is not robust.

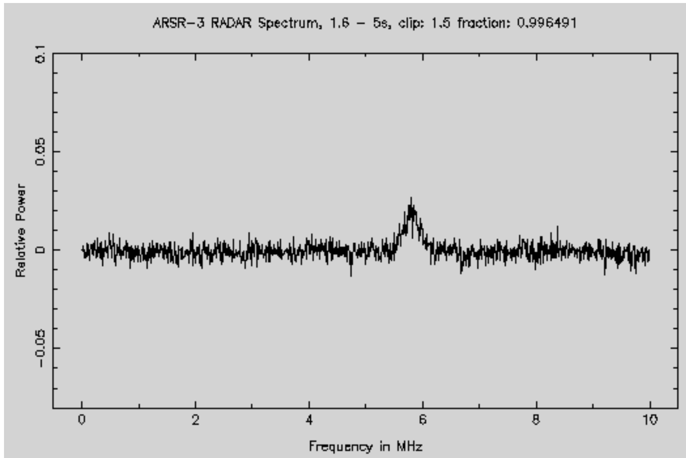

Figure 13. Spectrum with data blanked when a pulse was detected above a level of 1.5 units on the intensity scale shown in Figures 8, 9, and 14. The spectrum is integrated between 1.6 and 5 seconds into the data as it was in Figure 12. The intensity scale is in units of telescope system noise power.

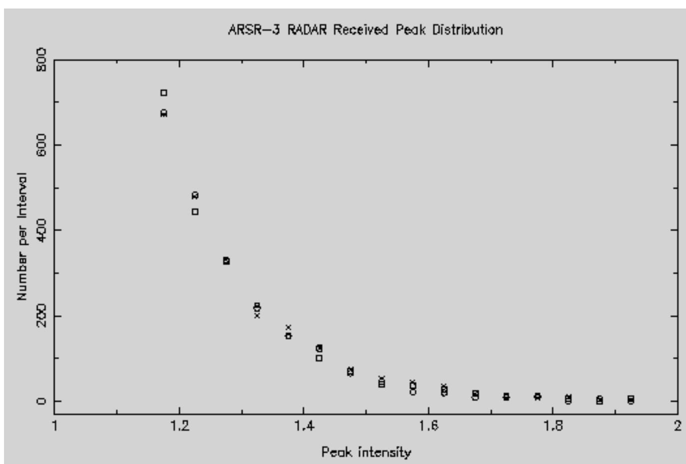

Figure 14. Distribution of measured intensity peaks in the data set after filtering as described in connection with Figures 2 and 3. The horizontal scale peak intensity of 1.0 corresponds to 0 dB on the vertical axes of Figures 8 and 9. The square, X, and circle correspond to frequency domain filter center frequencies of 4.7, 5.84 (radar frequency), and 6.5 MHz, respectively.

Figure 15 shows an integration over the 0.3 seconds when the radar beam was pointed close to the GBT using detected pulse blanking only. About 25 db of radar signal rejection was achieved, as can be seen in a comparison with Figure 13, but the low-amplitude pulses that slip under the detection threshold produced an unacceptable radar signal in the spectrum.

Detected pulse blanking probably does have a place in radar rejection, in combination with time window blanking, for rejecting transient pulse reflections that fall outside of the selected time window.

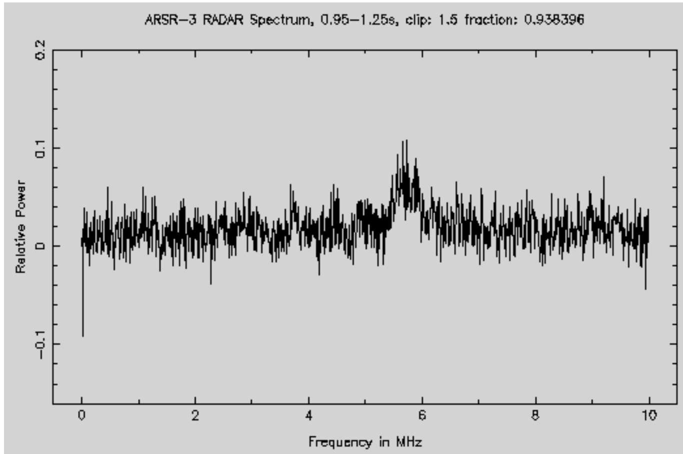

Figure 15. Spectrum with data blanked when a pulse was detected above a level of 1.5 units on the intensity scale shown in Figures 8, 9, and 14. The spectrum was integrated between 0.95 and 1.25 seconds into the data as in Figures 10 and 11. The intensity scale is in units of telescope system noise power. Note the change in vertical scale from previous figures.

Preliminary Conclusions

From this initial analysis of a small bit of radar data there are a number of points learned that will affect our work on mitigating RFI at the GBT with blanking and canceling techniques:

1. To observe redshifted hydrogen near the radar frequency, simply blanking the receiver when the radar beam passes over Green Bank is not sufficient. A more complex technique of isolating echo-free data between radar pulses is required.

2. Reflections from the highest terrain around Green Bank can produce a stronger signal than the more direct signal path from distant transmitters to the GBT.

3. Any RFI canceling techniques will need to account for multi-path signal propagation arriving from a wide range of azimuths and with differential delays of more than 100 microseconds.

4. Time window blanking does appear to be quite effective, and a large fraction of the time between radar pulses can be used for high sensitivity spectral line measurements.

5. Detected pulse blanking is not a usable technique on its own, but it can be used to reject moderately strong, long-delay pulse reflections that fall outside of the selected blanking time window.